# The Circadian Molecular Clock Regulates Adult Hippocampal Neurogenesis by Controlling the Timing of Cell-Cycle Entry and Exit

Pascale Bouchard-Cannon,[1] Lucia Mendoza-Viveros,[1] Andrew Yuen,[1] Mads Kærn,[2,*] and Hai-Ying M. Cheng[1,*]
[1]Department of Biology, University of Toronto Mississauga, 3359 Mississauga Road, Mississauga, ON L5L 1C6, Canada
[2]Ottawa Institute of Systems Biology, Department of Cellular and Molecular Medicine, and Department of Physics, University of Ottawa, 451 Smyth Road, Ottawa, ON K1H 8M5, Canada
*Correspondence: mkaern@uottawa.ca (M.K.), haiying.cheng@utoronto.ca (H.-Y.M.C.)
http://dx.doi.org/10.1016/j.celrep.2013.10.037

## SUMMARY

The subgranular zone (SGZ) of the adult hippocampus contains a pool of quiescent neural progenitor cells (QNPs) that are capable of entering the cell cycle and producing newborn neurons. The mechanisms that control the timing and extent of adult neurogenesis are not well understood. Here, we show that QNPs of the adult SGZ express molecular-clock components and proliferate in a rhythmic fashion. The clock proteins PERIOD2 and BMAL1 are critical for proper control of neurogenesis. The absence of PERIOD2 abolishes the gating of cell-cycle entrance of QNPs, whereas genetic ablation of *bmal1* results in constitutively high levels of proliferation and delayed cell-cycle exit. We use mathematical model simulations to show that these observations may arise from clock-driven expression of a cell-cycle inhibitor that targets the cyclin D/Cdk4-6 complex. Our findings may have broad implications for the circadian clock in timing cell-cycle events of other stem cell populations throughout the body.

## INTRODUCTION

Although neurogenesis (the birth of new neurons) is most active and widespread during embryonic development when the CNS is established, only restricted subregions of the postnatal mammalian brain retain the potential to generate new neurons. One of these neurogenic niches is the subgranular zone (SGZ) of the hippocampal dentate gyrus (DG), which contains a quiescent pool of stem cell-like neural stem/progenitor cells (NSPCs) (Altman and Das, 1965). Throughout adulthood, some of these NSPCs, or type 1 cells, will become activated and enter the cell cycle, undergoing a series of proliferative and differentiative events to eventually give rise to newborn DG granule neurons (Seri et al., 2001). This process involves the sequential generation of a pool of transient amplifying neural progenitors (ANPs

or type 2a/2b cells), terminally committed neuroblasts (type 3 cells) in which $G_0$ has been reinstated, and fully differentiated postmitotic neurons. In rodents, adult hippocampal neurogenesis is highly dynamic and modulated by stimuli such as exposure to enriched environments (Kempermann et al., 1997), voluntary exercise (van Praag et al., 1999), aging (Kuhn et al., 1996), and pathological insults to the brain (Parent et al., 1997). Although the functional relevance of adult hippocampal neurogenesis remains to be fully elucidated, it is generally believed to play an important role in higher cognitive function (e.g., learning and memory) and repair following traumatic brain injury.

The mechanisms that control if and when quiescent NSPCs, or QNPs, of the adult SGZ leave their dormant ($G_0$) state to initiate neurogenesis are not fully elucidated (Marqués-Torrejón et al., 2013; Song et al., 2012; Mira et al., 2010). Furthermore, once a QNP enters the cell cycle, it is not clear which processes are in play to ensure that the appropriate number of cell divisions will occur during execution of the neurogenic program. However, one possible mechanism is the circadian clock, which evolved to provide temporal coordination of many behavioral and physiological processes according to the demands of a 24 hr cyclic environment. The molecules that constitute the circadian clock machinery are expressed in many cell types throughout the mammalian body, including the central oscillators of the hypothalamic suprachiasmatic nucleus (SCN) and peripheral oscillators elsewhere that are coordinated by the SCN. These molecular components interact in transcription/translation feedback loops to drive 24 hr rhythms of clock-controlled gene expression.

Two key players in the circadian clock network are BMAL1, a transcription factor that promotes circadian transcription of E-box-containing genes, and *per2*, an E-box-regulated gene whose protein product feedback inhibits BMAL1-mediated transcription (and thus its own expression). Both *bmal1* and *per2* are necessary to sustain circadian rhythms in mammals (Zheng et al., 1999; Bunger et al., 2000). Despite evidence showing that the circadian clock can be coupled to proliferation and cell-cycle control in a number of biological systems (Geyfman et al., 2012; Dong et al., 2010), there is a dearth of information related to its potential role in adult hippocampal neurogenesis.
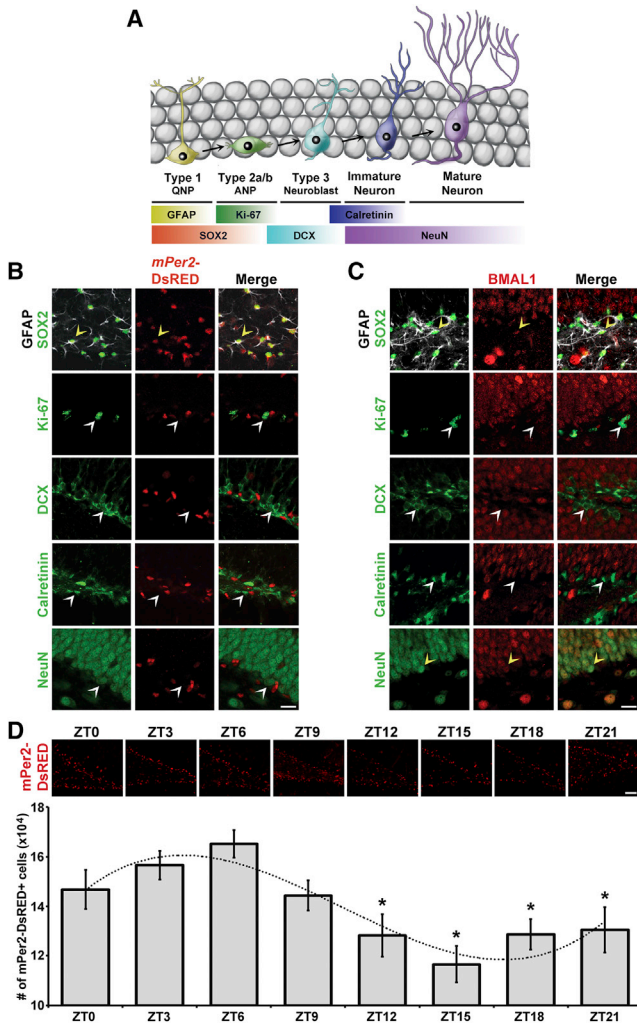
**Figure 1. A Functional Circadian Clock Exists within the Adult Murine SGZ**

(A) Illustration of the different stages of neurogenesis in the adult SGZ, including the expression of stage-specific markers.

(B and C) Colocalization of (B) *mPer2*-DsRED or (C) BMAL1 with stage-specific markers of neurogenesis at ZT 3. White arrowheads denote lack of colocalized expression between DsRED (red) or BMAL1 (red) and the stage-specific marker (green); yellow arrowheads indicate colocalized expression. GFAP is pseudocolored in white. Scale bar, 20 μm.

(D) *mPer2*-DsRED expression in the SGZ across the circadian cycle. Forty-day-old mice were dark-adapted for 2 days prior to tissue harvest at the indicated ZT. Scale bar, 50 μm. The y axis represents the number of *mPer2*-DsRED-expressing cells per mm$^3$ of SGZ. Values are given as mean ± SEM; n = 4–6 animals per time point. The data were best fitted with a sine curve. *p < 0.05 versus ZT 6.

See also Figure S1.

To explore a possible connection between the circadian clock and adult neurogenesis, we characterized the expression of core clock genes at different stages of neurogenesis in the murine SGZ, and investigated the effects of *bmal1* and *per2* ablation on cellular proliferation and the timing of cell-cycle events. Moreover, simulations of a modified mathematical model describing

the coupling of the circadian clock and the cell cycle (Gérard and Goldbeter, 2012) were able to reproduce our empirical observations, and provide a mechanistic framework to understand the influence of the circadian clock on cell-cycle dynamics in the SGZ. Importantly, our study shows that a circadian clock exists within QNPs to time their entry into the cell cycle, and that reestablishment of the quiescent state during neuronal differentiation is delayed in the absence of the circadian clock.

## RESULTS

### The Molecular Clock Is Present in NSPCs of the Adult Murine SGZ

To examine the role of the circadian clock in adult hippocampal neurogenesis, we first mapped the expression of several core clock genes in the various cell types of the SGZ as delineated by the coexpression of stage-specific markers (Figure 1A). *mPeriod2* expression was monitored using the bacterial artificial chromosome (BAC) transgenic mouse strain *mPer2*-DsRED, which expresses the DsRED fluorophore under the control of the full-length *mPer2* gene promoter (Cheng et al., 2009). Within the SGZ, DsRED expression was detected in all type 1 NSPCs (Sox2$^+$GFAP$^+$) (99.6% ± 0.2%) (Figures 1B and S1E). Proliferating (Ki67$^+$) cells of the SGZ expressed very low levels of DsRED (Figures 1B, S1C, and S1D). Furthermore, DsRED expression was undetectable in cells representing the later stages of neurogenesis, including the doublecortin-positive (DCX$^+$) type 2b/3 precursors and the calretinin-positive immature neurons, as well as mature (NeuN$^+$) granule neurons of the DG (Figure 1B).

To examine the expression of BMAL1 and *mPeriod1* in the SGZ, we used a BMAL1-specific antibody (Figure 1C) and a sister reporter BAC transgenic mouse strain that expresses the VENUS fluorophore under the control of the *mPer1* gene promoter (Figure S1B) (Cheng et al., 2009), respectively. Like DsRED, BMAL1 and VENUS were detected in all type 1 NSPCs, but their levels were strongly suppressed in proliferating cells (Figures S1C and S1D). In addition, VENUS was expressed in the subset of DCX$^+$ cells with blast-like morphology (likely postmitotic type 3 neuroblasts), as well as all NeuN$^+$ mature DG granule neurons (Figure S1B). BMAL1, on the other hand, was undetectable in both DCX$^+$ and calretinin$^+$ populations, and reappeared only in mature neurons (Figure 1C). Further analysis revealed that all DsRED$^+$ cells of the SGZ coexpressed other components of the core clock machinery, including BMAL1, *mPeriod1*, CRY2, and CLOCK (Figure S1A). Finally, as evidence that the molecular clock is functional in the SGZ, we sought to establish a circadian rhythm of clock gene expression. Using the *mPer2*-DsRED model, we found that the number of DsRED$^+$ cells in the SGZ fluctuated as a function of time-of-day (Figure 1D), peaking in the early to mid-subjective day and reaching trough levels in the early to mid-subjective night. Together, the data indicate that a functional circadian clock exists within type 1 NSPCs of the SGZ.

### Cell Proliferation in the Adult SGZ Is Rhythmic and Controlled by the Molecular Clock

We addressed the functional relevance of the circadian clock on adult hippocampal neurogenesis by examining its effects on
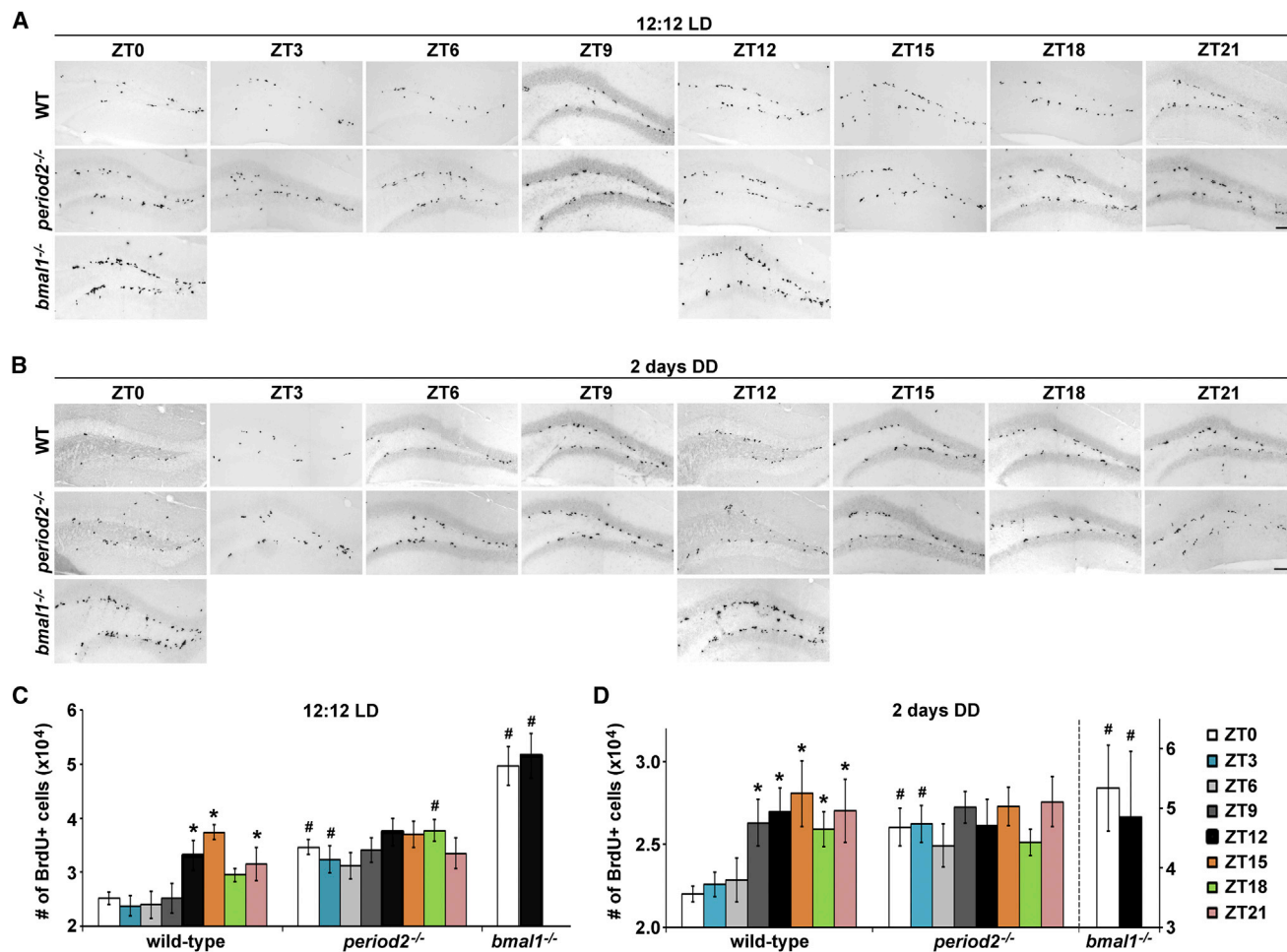
**Figure 2. Time-of-Day-Dependent Cellular Proliferation in the Murine SGZ Is Ablated in the Absence of mPeriod2 or Bmal1**

(A and B) Forty-day-old wild-type, *period2*$^{-/-}$, and *bmal1*$^{-/-}$ mice were either (A) maintained on a 12:12 LD cycle or (B) dark-adapted for 2 days prior to receiving a BrdU injection at the indicated ZT. Tissues were harvested (A) 6 hr or (B) 3 hr postinjection. Representative photomicrographs of BrdU$^+$ cells in the SGZ are shown. Scale bar, 100 μm.

(C and D) Number of BrdU$^+$ cells per mm$^3$ of SGZ for mice that were (C) maintained on an LD cycle or (D) dark-adapted prior to BrdU injection at the indicated ZT. Note that the y axis scale (D, right) is different for *bmal1*$^{-/-}$ mice. Values are given as mean ± SEM; n = 4–9 animals per time point. $^#$p < 0.05 versus wild-type; *p < 0.05 versus ZT 0 within the same genotype.

See also Figure S2.

cellular proliferation in the SGZ. Dark-adapted 40-day-old wild-type mice were injected with the thymidine analog bromodeoxyuridine (BrdU) every 3 hr across the 24 hr circadian cycle. Our results show that the number of BrdU$^+$ cells in the wild-type SGZ varied significantly as a function of time-of-day (Figures 2B and 2D), such that higher levels of proliferation were observed in the subjective night compared with the early to mid-subjective day. We obtained similar results when we examined proliferation in wild-type mice that were maintained on a fixed 12 hr light/12 hr dark (LD) cycle at the time of BrdU injection (Figures 2A and 2C). The fold difference in peak-to-trough levels of BrdU$^+$ cells was between 1.3 (for complete darkness [DD]) and 1.6 (for LD). Importantly, these data demonstrate that there is indeed a circadian rhythm of cell proliferation in the adult SGZ.

Next, we examined the effects of *Bmal1* or *Per2* gene ablation on SGZ cell proliferation. In the absence of *Per2*, rhythms in SGZ

cell proliferation under both DD and LD conditions were abolished such that the numbers of BrdU$^+$ cells at all time points approached the peak values observed in wild-type controls (Figure 2). Under both DD and LD conditions, *bmal1*$^{-/-}$ mice exhibited a striking increase in the total number of BrdU$^+$ cells in the SGZ at Zeitgeber time 0 (ZT 0) and ZT 12 (1.9- to 2.4-fold versus wild-type), and there was no statistical difference between the two time points (Figure 2).

Given that individual *per2*$^{-/-}$ mice may exhibit varying behavioral phenotypes, including a short circadian period and arrhythmicity under DD (Zheng et al., 1999), we wanted to rule out the possibility that dispersion or discrepancies in the phase of individuals within this genotype contributed directly to the apparent lack of rhythms in SGZ cell proliferation. In an independent experiment, wheel-running activity rhythms were recorded for wild-type and *per2*$^{-/-}$ mice and used to predict circadian time
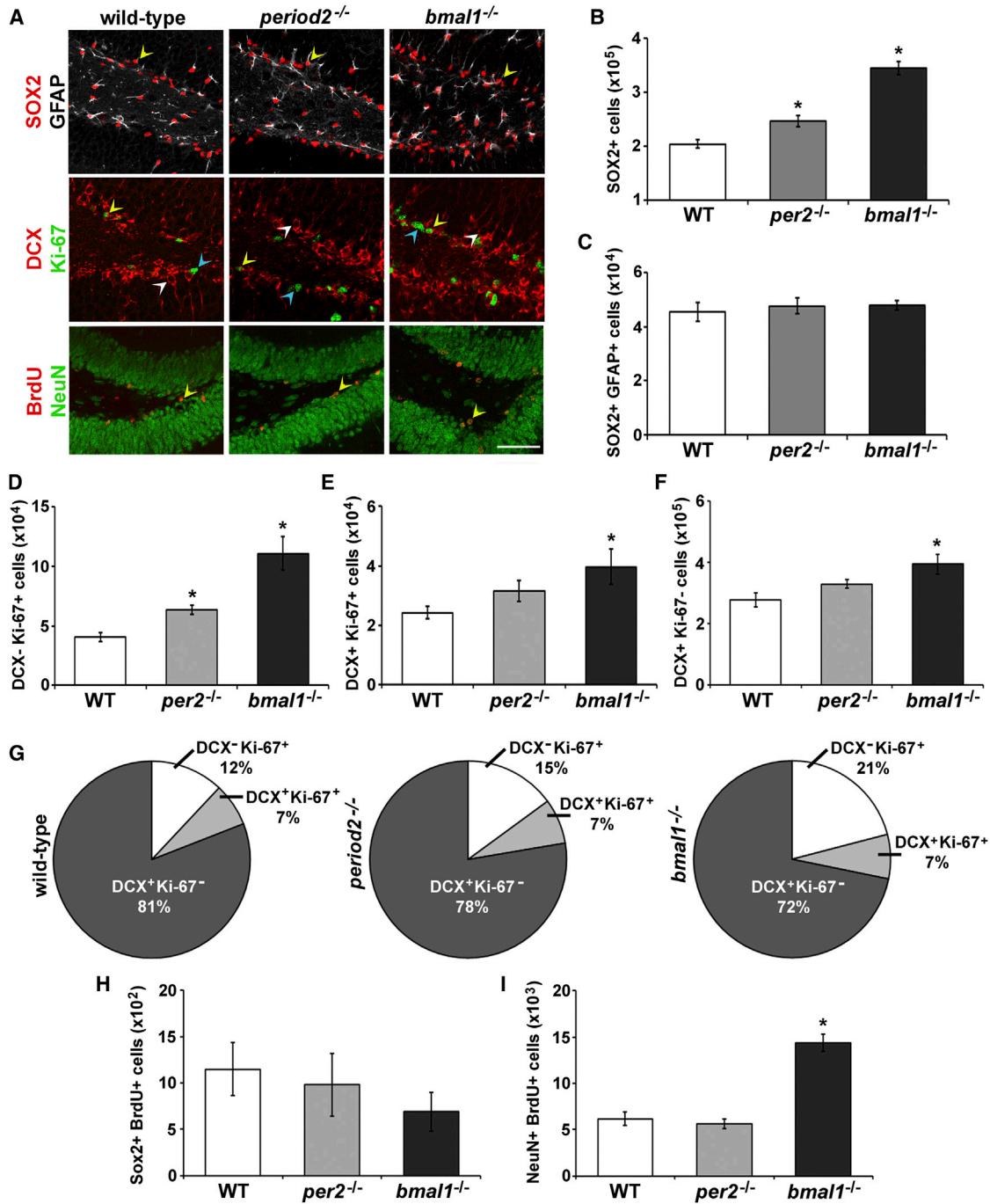
**Figure 3. Proper Regulation of Adult Hippocampal Neurogenesis Is Disrupted in the Absence of mPeriod2 or Bmal1**

(A) Expression of neurogenic markers in the SGZ of wild-type, $per2^{-/-}$, and $bmal1^{-/-}$ mice. For the top and middle rows, 40-day-old mice had been dark-adapted for 2 days prior to tissue harvest at ZT 3. For the bottom row, starting at 40 days of age, mice received daily injections of BrdU at ZT 2 for 7 consecutive days and tissues were harvested 30 days after the first injection. Representative photomicrographs are shown. GFAP is pseudocolored in white. Yellow arrowheads indicate colocalization; blue and white arrowheads indicate lack of colocalization. Scale bars, 100 μm.

(B–F) Quantification of cells expressing the various neurogenic markers. The y axis indicates the number of cells per mm³ of SGZ. Values are given as mean ± SEM; n = 4 per genotype.

(B) Number of Sox2⁺ cells, which include both type 1 and type 2a cells.

(C) The Sox2⁺GFAP⁺ pool represents type 1 cells only.

(D) DCX⁻Ki67⁺ cells represent all proliferating (type 1 and type 2a) cells, excluding DCX⁺ type 2b precursors.

(E) DCX⁺Ki67⁺ cells represent proliferating type 2b precursors.

*(legend continued on next page)*

0 (CT 0) and CT 12 under free-running conditions (Figure S2A). All *per2*^{-/-} mice (16/16) tested remained rhythmic, with a period of ~22 hr, after 4 days in DD. Whereas wild-type mice showed a significant difference in the number of BrdU+ cells in the SGZ at CT 0 and CT 12, the *per2*^{-/-} mice did not (Figures S2A and S2B). For both genotypes, the number of BrdU+ cells was elevated compared with animals that had not been exposed to a running wheel (Figure 2), consistent with previous reports indicating the stimulatory effects of voluntary exercise on hippocampal neurogenesis (van Praag et al., 1999).

In total, these data reveal that cell proliferation in the adult murine SGZ is rhythmically controlled by the circadian clock, and that *Per2* and *Bmal1* critically regulate rhythms and overall levels of proliferation in this particular neurogenic niche.

### Ablation of *Per2* or *Bmal1* Increases the Number of ANPs or Neuroblasts without Altering the Pool of NSPCs

To further characterize the effects of *Per2* or *Bmal1* gene ablation on adult hippocampal neurogenesis, we quantitated the number of cells in different stages of neurogenesis in the SGZ of 40-day-old wild-type, *per2*^{-/-}, and *bmal1*^{-/-} mice. All genotypes possessed a comparable number of type 1 (Sox2+GFAP+) NSPCs in the SGZ (Figures 3A, top row, and 3C). However, the total number of Sox2+ cells (consisting of both type 1 NSPCs and type 2a ANPs) was significantly greater in both *bmal1*^{-/-} and *per2*^{-/-} mice relative to wild-type controls, with *bmal1*^{-/-} mice showing the larger enhancement (Figures 3B and S3, first row). These data rule out the possibility that the increase in BrdU+ cells in the mutant strains was simply a by-product of a larger, preexisting pool of type 1 NSPCs rather than an authentic increase in the proliferative capacity of *bmal1*- or *per2*-deficient neural progenitors. Along these lines, we found that the number of actively proliferating cells in the type 1/2a pools (Ki67+DCX-) was significantly enhanced in *bmal1*^{-/-} and *per2*^{-/-} mice relative to wild-type controls (Figures 3A, middle row, and 3D).

Next, we assessed potential changes in the type 2b/3 pools. In *per2*^{-/-} SGZ, the numbers of proliferating type 2b (Ki67+DCX+) (Figure 3E) and postmitotic type 3 (Ki67-DCX+) (Figure 3F) cells were similar to those of wild-type controls. However, there was a marked increase in both type 2b and type 3 pools in the SGZ of *bmal1*^{-/-} mice (Figures 3E and 3F). Notably, when compared with wild-type and *per2*^{-/-} SGZ, *bmal1*^{-/-} SGZ had a higher proportion of proliferating type 1/2a (Ki67+DCX-) to type 2b (Ki67+DCX+) cells (3:1 versus ~2:1), suggesting that the expansion of the type 2a pool is greater relative to the type 2b pool in these animals (Figure 3G).

Lastly, we examined the integration of newborn neurons into the DG by quantitating the retention of BrdU+ cells 30 days after the start of a 7-day schedule of daily BrdU injections (Figure S3, bottom row). The number of BrdU label-retaining cells (LRCs) in the DG that coexpressed the mature neuronal marker NeuN was comparable between wild-type and *per2*^{-/-} mice, as expected given the lack of increase in the type 3 cell population (Figures 3A, bottom row, and 3I). In contrast, *bmal1*^{-/-} mice had a significantly greater number of BrdU+NeuN+ cells in the DG (Figures 3A, bottom row, and 3I). However, there was no difference in the self-renewal of neural progenitors among all genotypes, as indicated by the numbers of BrdU+Sox2+ cells in the SGZ (Figure 3H). Collectively, these data reveal that *Per2* and *Bmal1* are critical for restricting the expansion of the rapidly dividing uncommitted and committed neural precursors in the SGZ, with *Bmal1* playing an additional role in buffering against overproduction of newborn granule neurons.

### *Bmal1* and *Period2* Time the Events of the Cell Cycle in the Adult SGZ

To explore the underlying causes of aberrant cell proliferation in the SGZ of our mutant mice, we turned our attention to the relationship between the circadian clock and cell-cycle progression. First, we asked whether the entry of QNPs into the cell cycle is regulated in a circadian fashion. Using S phase as a marker of the cell cycle, we injected dark-adapted mice with BrdU at either ZT 0 or ZT 12 and immunostained harvested tissues for BrdU, Sox2, and GFAP (Figure 4A). In wild-type controls, there was a ~2.5-fold increase in the proportion of BrdU+Sox2+GFAP+ cells within the type 1 pool at ZT 12 relative to ZT 0 (Figure 4B). These data reveal that QNPs enter the cell cycle in a circadian-dependent fashion. In *per2*^{-/-} SGZ, the proportion of BrdU+Sox2+ GFAP+ cells was indistinguishable between the two time points examined, and was intermediate between wild-type values obtained at ZT 0 and ZT 12 (Figure 4B). We obtained similar results when we assessed cell-cycle entrance in wild-type and *per2*^{-/-} mice that had been housed in wheel cages and injected with BrdU based on behaviorally predicted CTs (Figure S2C). Thus, *per2* expression appears to be required for circadian-regulated entrance of QNPs into the cell cycle. More strikingly, in the absence of *bmal1*, there was a profound increase in the proportion of BrdU+Sox2+GFAP+ cells at both ZT 0 and ZT 12 relative to wild-type controls, and no significant difference between the two time points (Figure 4B). These results reveal that *bmal1* is critical for restricting QNP activation and entrance into the cell cycle.

Previous studies have suggested that ANPs undergo ~2.3 divisions before withdrawing from the cell cycle and converting to neuroblasts (Encinas et al., 2011). To examine a potential role of BMAL1 and PER2 in cell-cycle exit, we quantified the rate of cell-cycle exit by determining the proportion of BrdU+ cells that ceased to express Ki-67 24 hr postinjection (Figure 4C). Our results indicate that the percentage of cells that exited the cell cycle was similar between wild-type and *per2*^{-/-} mice (~39% versus ~43%), but was significantly reduced in *bmal1*^{-/-}

---

(F) DCX+Ki67- cells represent all postmitotic type 3 neuroblasts.

(G) Relative abundance of proliferating type 1/2a (DCX-Ki67-), type 2b (DCX+Ki67+), and type 3 (DCX+Ki67-) cells in the SGZ of wild-type, *per2*^{-/-}, and *bmal1*^{-/-} mice.

(H and I) Quantification of BrdU label-retaining (H) Sox2+ neural progenitors in the SGZ and (I) NeuN+ newborn neurons in the granule cell layer of wild-type, *per2*^{-/-}, and *bmal1*^{-/-} mice. The y axis indicates the number of double-positive cells per mm$^3$. Values are given as mean ± SEM; n = 4–5 per genotype. *p < 0.05 versus wild-type.

See also Figure S3.
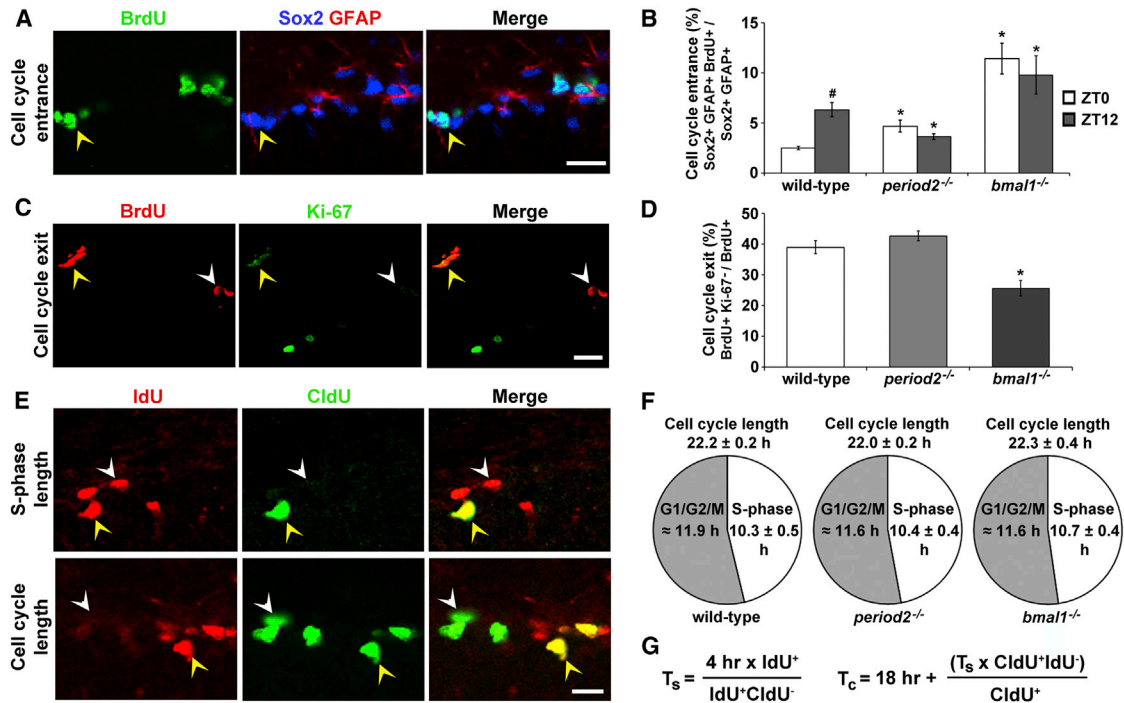
**Figure 4. The Circadian Clock Regulates Cell-Cycle Entry and Exit without Altering Cell-Cycle Kinetics**

(A and B) Cell-cycle entrance analysis. Forty-day-old mice were dark-adapted for 2 days and injected at ZT 0 or ZT 12 with BrdU prior to tissue harvest 3 hr postinjection.

(A) Representative photomicrographs of BrdU, Sox2, and GFAP immunoreactivity in the SGZ of wild-type mice.

(B) Proportion of type 1 cells that entered the cell cycle at ZT 0 and ZT 12, calculated as the number of Sox2$^+$GFAP$^+$BrdU$^+$ cells / the total number of Sox2$^+$GFAP$^+$ cells × 100%.

(C and D) The index of cell-cycle exit was determined by injecting 40-day-old mice with BrdU at ZT 12 and harvesting tissues 24 hr postinjection.

(C) Representative photomicrographs of BrdU and Ki-67 immunoreactivity in the SGZ of wild-type mice.

(D) The percentage of cells exiting the cell cycle was calculated as the number of BrdU$^+$Ki67$^-$ cells / total number of BrdU$^+$ cells × 100%.

(E–G) Cell-cycle kinetics. On the second day of DD, 40-day-old mice were injected with IdU at ZT 8 and received a second injection of CldU either 4 hr (E, top row) or 18 hr (E, bottom row) later. Tissues were harvested 45 min after CldU injection.

(E) Representative photomicrographs of IdU and CldU immunoreactivity in the SGZ of bmal1$^{-/-}$ mice for the determination of (top row) S phase length and (bottom row) cell-cycle length.

(F) Schematic of the calculated lengths of S phase and cell cycle for wild-type, per2$^{-/-}$, and bmal1$^{-/-}$ mice. The combined G1/G2/M length was estimated as the difference between cell-cycle length and S phase duration.

(G) Equations used to calculate the S phase length (T$_s$) and the cell-cycle length (T$_c$).

(A, C, and E) White arrowheads denote lack of colocalization, and yellow arrowheads indicate colocalized expression. Scale bars, 20 μm (A and C) and 10 μm (E).

(B, D, and F) Values are given as mean ± SEM; n = 4–6 per genotype. *p < 0.05 versus wild-type; #p < 0.05 versus ZT 0.
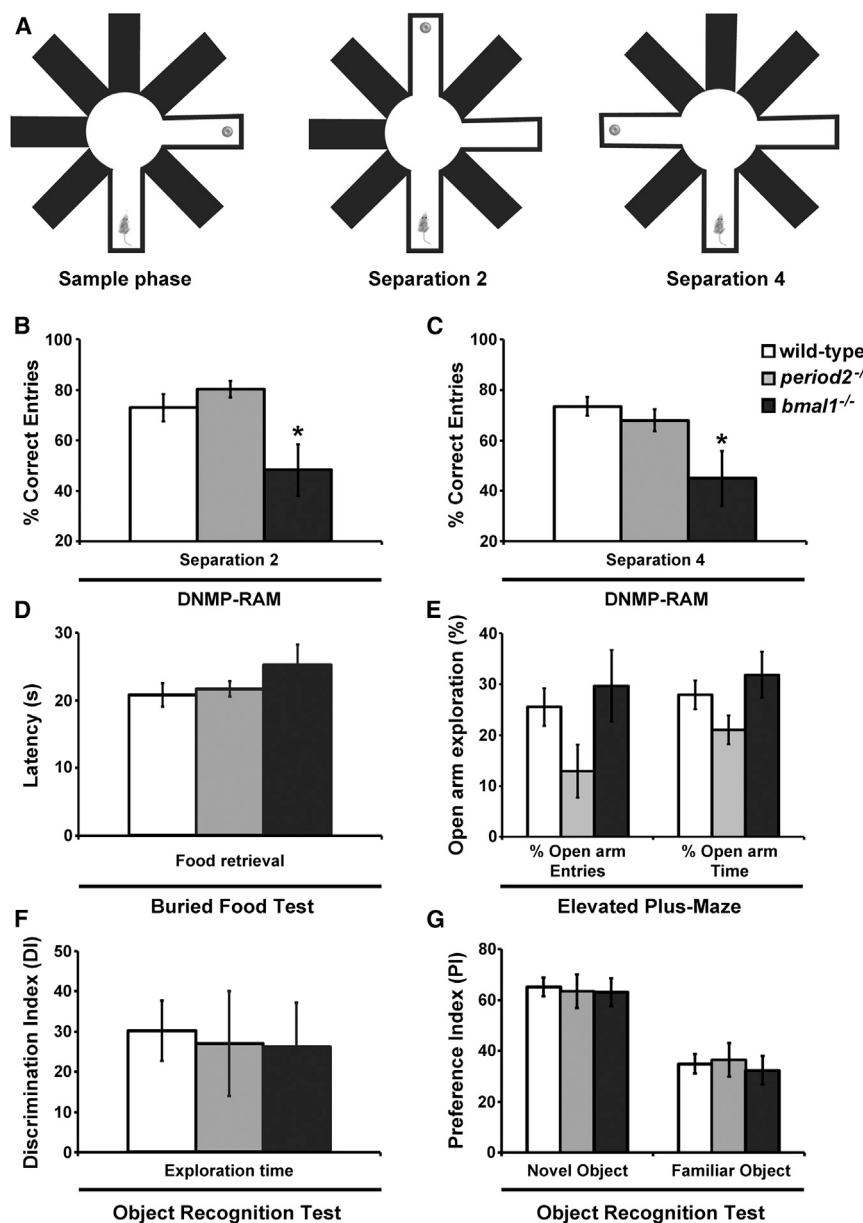
See also Figure S4.

mice (∼26%) (Figure 4D). This suggests to us that in the absence of *bmal1*, proliferating cells in the SGZ undergo more rounds of cell division than wild-type controls before withdrawing from the cell cycle. Given the increase in the relative proportion of type 2a to type 2b cells in *bmal1*$^{-/-}$ SGZ (Figure 3G), the additional divisions might occur within the type 2a (Sox2$^+$) pool. It is important to note that from these data, we cannot conclude precisely how many division events take place in wild-type cells as opposed to *bmal1*$^{-/-}$ cells. A quantitative analysis of the number of cell divisions would require additional experiments using multiple thymidine analogs with varying injection intervals.

Lastly, we examined cell-cycle kinetics in the SGZ of our wild-type and mutant strains. We determined the lengths of the S phase and cell cycle by spacing the injections of two thymidine analogs, IdU and CldU, either 4 hr or 18 hr apart, respectively

(Figure 4E), and using the equations provided (Figure 4G). Importantly, ablation of *bmal1* or *per2* did not significantly impact the total cell-cycle length or S phase duration (Figure 4F).

Studies have shown that adult hippocampal neurogenesis is coupled to angiogenesis through shared growth factors (Jin et al., 2002). To rule out the possibility that the neurogenic phenotype in *per2*$^{-/-}$ and *bmal1*$^{-/-}$ mice is indirectly related to factors that promote angiogenesis, we examined potential differences in vascularization in the hippocampus. Using CD31 as a marker of vascular endothelial cells, we found that there was no significant difference in the degree of vascularization in either the granule cell layer or the hilus of all three genotypes (Figure S4).

Collectively, the data reveal that *Period2* is essential for temporally restricting cell-cycle entry of type 1 NSPCs. In

**A**

Sample phase      Separation 2      Separation 4

**B** — DNMP-RAM, Separation 2, % Correct Entries

**C** — DNMP-RAM, Separation 4, % Correct Entries

□ wild-type
▨ period2⁻/⁻
■ bmal1⁻/⁻

**D** — Buried Food Test, Food retrieval, Latency (s)

**E** — Elevated Plus-Maze, Open arm exploration (%), % Open arm Entries / % Open arm Time

**F** — Object Recognition Test, Exploration time, Discrimination Index (DI)

**G** — Object Recognition Test, Novel Object / Familiar Object, Preference Index (PI)

**Figure 5. Ablation of *bmal1* Selectively Impairs Performance on Hippocampal Neurogenesis-Dependent Learning Tasks**

(A) Representative schematic of the DNMP-RAM test. In the sample phase (left), mice are placed in the start arm and allowed to retrieve a food pellet (gray circle) in the sample arm. In the test phase (middle and right), mice are placed in the start arm and given the choice of a familiar arm and a novel (correct) arm that has been baited with a food pellet. The familiar and novel arms are separated by two (middle) or four (right) arms. Black indicates regions that have been blocked off and are inaccessible to the mouse.

(B and C) DNMP-RAM test. The y axis indicates the percentage of correct entries in (B) separation 2 and (C) separation 4 tests. Values are given as mean ± SEM; n = 12 wild-type, n = 17 *per2*⁻/⁻, n = 9 *bmal1*⁻/⁻. *p < 0.05 versus wild-type.

(D) Buried-food test. The y axis indicates the latency (s) to retrieve a buried food pellet.

(E) Elevated plus maze. The y axis indicates the percentage of entries or time spent in the open arm during a 5 min period on the elevated plus maze.

(F and G) Object-recognition test. The y axes indicate the (F) discrimination index and (G) preference index calculated using the exploration times for the novel object and the familiar object.

(D–G) Values are given as mean ± SEM; n = 6 per genotype.

See also Figure S5.

contrast, *Bmal1* has a dual role in limiting both the proportion of type 1 NSPCs that leave quiescence and enter into the proliferative state, and the number of cell divisions that occur before neural precursors withdraw permanently from the cell cycle on their path to terminal differentiation.

### Deregulated Hippocampal Neurogenesis in *bmal1*⁻/⁻ Mice Is Associated with Impaired Cognitive Function

The hippocampus is a vital structure for certain types of learning and memory formation. Recent studies have shown that adult neurogenesis in the DG plays a critical role in spatial discrimination or pattern separation (Clelland et al., 2009). To examine the cognitive repercussions of altered hippocampal neurogenesis in *per2*⁻/⁻ and *bmal1*⁻/⁻ mice, we tested these mice on a battery of

hippocampal-dependent and -independent behavioral paradigms. The delayed nonmatching to place (DNMP) radial eight-arm maze (RAM) task (Figure 5A), which has been shown to rely on adult hippocampal neurogenesis, was used to assess pattern separation-dependent memory (Clelland et al., 2009). In the test phase of the DNMP-RAM task, mice were given a choice between a familiar (sample) arm and a novel (correct, food-baited) arm, which were separated by two (S2) or four (S4) arms (Figure 5A). *Per2*⁻/⁻ mice were similar to wild-type controls in their ability to discriminate between locations that were spatially close together (S2) (Figures 5B, S5A, and S5C) or far apart (S4) (Figures 5C, S5B, and S5C). Surprisingly, *bmal1*⁻/⁻ mice performed significantly worse than wild-types under both the S2 and S4 settings (Figures 5B, 5C, and S5A–S5C). A possible explanation for this is that there exists a restricted window within which enhanced adult neurogenesis is beneficial for learning. Excessive (or deregulated) neurogenesis beyond the limits of this range might potentially interfere with hippocampal-dependent learning. Importantly, the results from the DNMP-RAM task were due to neither a deficit in olfaction nor altered anxiety in *bmal1*⁻/⁻ mice, since their performance on a buried-food test (olfaction) (Figure 5D) and the elevated plus maze (anxiety)

(Figures 5E and S5D) was comparable to that of wild-type and *per2*−/− mice. Moreover, all three genotypes performed similarly well on a novel-object-recognition task, which examines short-term visual memory (Figures 5F–5G, S5E, and S5F). Given that the behavioral tests were performed on young mice (6–7 weeks old), it seems unlikely that the myriad of aging-related phenotypes exhibited by *bmal1*−/− mice, including arthropathy (Bunger et al., 2005), would account for their poor performance on the DNMP-RAM task, since most of these other phenotypes are not pathologically detectable until at least 10 weeks of age. Still, we do not rule out the possibility that factors other than (or in addition to) altered hippocampal neurogenesis in *bmal1*−/− mice contributed to their performance on behavioral tasks, for example, by affecting their motivation. Together, the data show that *bmal1* deficiency selectively impairs pattern-separation-dependent learning and memory, potentially as a result of altered adult hippocampal neurogenesis.

## Mathematical Simulations Reveal Cyclin-Dependent Kinase Inhibition as a Potential Link between the Circadian Clock and Cell-Cycle Entry and Exit

To explore potential mechanisms underlying the effects of *bmal1* and *per2* ablation on adult hippocampal neurogenesis, we turned to a computational model that was previously developed by Gérard and Goldbeter (2009, 2012) to investigate how circadian rhythms can influence cell-cycle progression. The model captures several known coupling interactions between the circadian clock and the cell cycle, including clock-driven expression of Wee1 and the cyclin-dependent kinase (CDK) inhibitor p21. Previous analyses have focused primarily on effects mediated by Wee1 under conditions of sustained cell proliferation caused by constant mitogen stimulation. Because of the known role of p21 in the maintenance of quiescence in adult mammalian forebrain neural stem cells (Kippin et al., 2005), we used the model to explore how partial and transient suppression of the circadian clock, through a Cyclin D/Cdk4-6 protein inhibitor such as p21, might impact cell-cycle entry and exit.

Only relatively minor modifications of the model were required to capture the empirical effects of *bmal1* and *per2* deletion on cell-cycle entry and exit. The original model assumed that BMAL1 represses p21 indirectly, based on observations in hepatocytes (Gréchez-Cassiau et al., 2008). Although this scenario establishes a circadian gating of cell-cycle entry, it cannot explain why *bmal1* ablation enhances cell proliferation in the SGZ. We therefore modified the model to test the alternative hypothesis that BMAL1 enhances the expression of a Cyclin D/Cdk4-6 protein complex inhibitor. Although our revised model labels this CDK inhibitor as p21 and assumes that BMAL1 activates its expression directly, as suggested by others (Laranjeiro et al., 2013), the molecular details are unclear. It is possible that inhibition of Cyclin D/Cdk4-6 involves other proteins, or that the circadian clock modulates this inhibition through other, indirect mechanisms.

Figures 6A and 6B illustrate the results of simulations mimicking the effect of mitogen stimulation of wild-type cells at ZT 0 and ZT 12, respectively. Prior to stimulation, the cell cycle was arrested at $G_0$, while levels of nuclear BMAL1 and p21 oscillated with a 24 hr period. Mitogen stimulation triggered cell-cycle

entry due to two effects: enhanced Cyclin D expression caused by AP1 activation, and a decline in p21 expression caused by partial suppression of the circadian clock. Because of the clock-driven oscillations in p21 levels, the time required for wild-type cells to be released from quiescence was strongly dependent on circadian clock phase at the time of mitogen stimulation. This phase dependency is further emphasized in Figure S6C, which shows the lag between mitogen stimulation and the first cell division for different stimulation ZTs. When the data were replotted according to the predicted ZT of the first M phase entrance, the timing of wild-type cells to enter M phase was clustered between ZT 0 and ZT 12 (Figure 6E).

To model the exit from the cell cycle, we assumed that cells gradually adapt to the mitogen such that the activation of AP1 and the partial suppression of the circadian clock diminish over time. This eventually leads to cell-cycle arrest as the rate of Cyclin D synthesis becomes too low to overcome clock-driven p21 expression. With the chosen values of model parameters, wild-type cells were able to complete either two or three divisions before withdrawing from the cell cycle (Figures 6A, 6B, and 6F). These division cycles, which occurred as clock-driven rhythms were being reestablished, had a periodicity of ∼19.7 ± 0.4 hr (Figure S6D).

Based on our model, clock-driven rhythms in p21 were abolished in the absence of *bmal1* (Figures 6D and S6B). Consequently, *bmal1*-deficient cells entered the cell cycle more quickly following mitogen stimulation (Figure S6C) and were able to complete four divisions before cell-cycle arrest was reestablished (Figures 6D, 6F, and S6B), irrespective of the ZT of mitogen stimulation. In contrast to wild-type cells, the timing of M phase entry of *bmal1*-deficient cells was not dependent on time-of-day (Figure 6E). The predicted cell-cycle period was similar to that of wild-type cells at ∼19.5 hr (Figure S6D). Importantly, these simulated effects of *bmal1* depletion are in line with our experimental data. First, BMAL1 impacts cell-cycle entry by modulating the mitogen stimulation threshold needed to trigger the release from quiescence (Figure 6G). The stimulation threshold arises from a complex interplay between the rate of Cyclin D and p21 expression, the timing of mitogen stimulation, and the level of clock repression. This is illustrated in Figures 6H and S6E, where the critical Cyclin D expression rate required to induce cell division is plotted as a function of the BMAL1 repression level at different rates of p21 expression. Notably, suppression of the circadian clock becomes an absolute requirement for cell-cycle entry when p21 expression is sufficiently high. Second, BMAL1 accelerates the withdrawal from the cell cycle by contributing to Cyclin D/Cdk4-6 suppression.

Interestingly, our model also provides a plausible mechanism to explain the effects of deleting the *mPer2* gene (Figures 6C and S6A). Specifically, in the circadian clock network model, the complete or partial loss of *period* gene function causes the oscillations in BMAL1 expression to slow down and uncouple from the normal 24 hr LD cycle (Figure 6C). This *period*-independent, sustained rhythm at the single-cell level could be due to a negative feedback loop exerted by BMAL1 on the expression of its gene (Leloup and Goldbeter, 2004). This notion, however, is not inconsistent with a loss of gating of cell-cycle entry at the population level. Although stimulated *Per2*-depleted cells
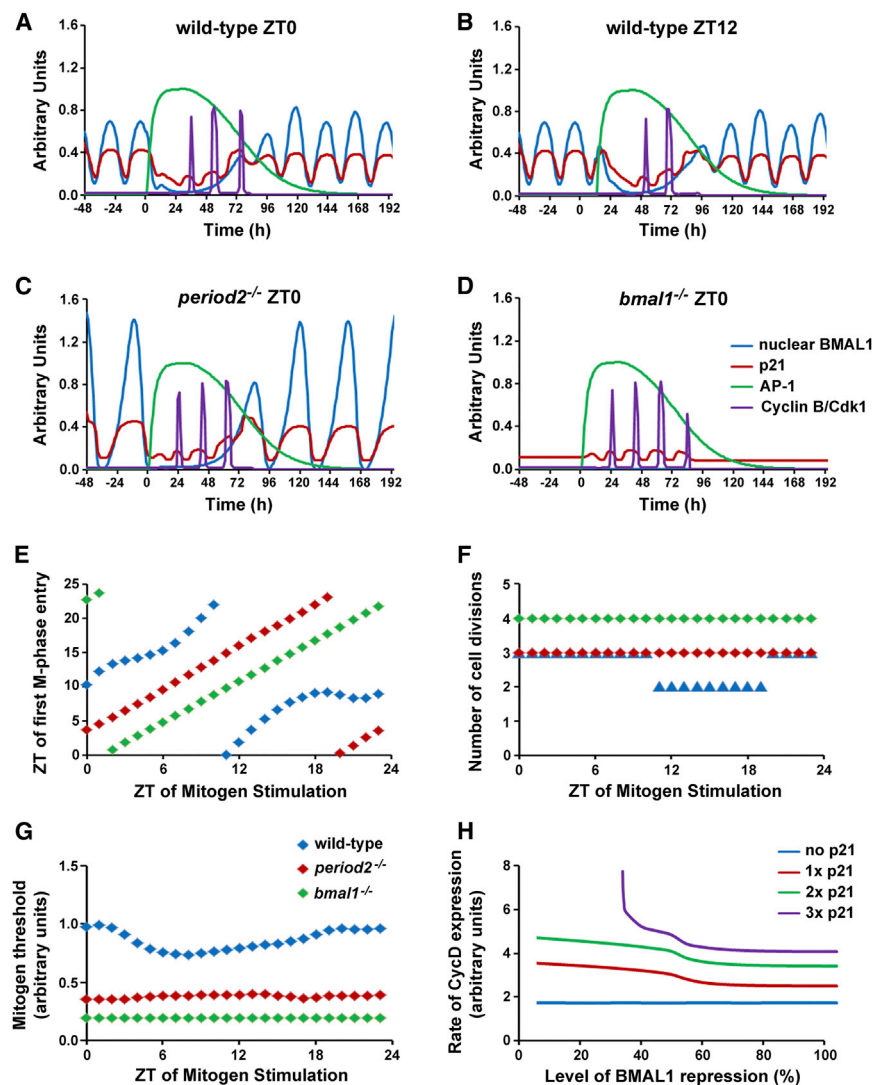
**Figure 6. Model Simulations of Cell-Cycle Entry and Exit following Transient Suppression of the Circadian Clock**

(A–D) Time series of nuclear BMAL1, AP1, and p21 levels, as well as cyclin B/Cdk1 activity, in (A and B) wild-type cells that were mitogen-stimulated at (A) ZT 0 or (B) ZT 12, and in (C) $per2^{-/-}$ and (D) $bmal1^{-/-}$ cells that were stimulated at ZT 0. The x axes represent time (hr), where ZT 0 is defined as time = 0. The y axes represent arbitrary units of expression or % activity (for cyclin B/Cdk1). Note that mitogen stimulation activates AP1 and downregulates p21 expression to temporarily release cells from quiescence. Wild-type cells complete two to three divisions (represented as spikes in cyclin B/Cdk1 activity) before withdrawing from the cell cycle. In contrast, clock-driven p21 expression is abolished in $bmal1^{-/-}$ cells, which complete four divisions prior to cell-cycle exit.

(E) Dependence of the timing of the first M phase entry on the time of mitogen stimulation. The x axis represents the ZT of mitogen stimulation. The y axis represents the ZT of the first M phase entry.

(F) Effects of *per2* or *bmal1* ablation on the number of cell divisions completed following mitogen stimulation. The x axis represents the ZT of mitogen stimulation.

(G) Dependence of the mitogen threshold for $G_0$ release on the time of mitogen stimulation. Note that in wild-type cells, there is a reduction in the mitogen threshold between ZT 6 and ZT 12, which makes it easier to enter the cell cycle at these times.

(H) The effects of repressing *bmal1* expression on the rate of Cyclin D expression required at ZT 0 to induce proliferation. Each curve represents a different level of basal p21 expression, where 1× denotes p21 levels used in the other simulations, and 2× and 3× denote increase in basal p21 levels by 2- or 3-fold, respectively. Note that for the 3× curve, there is no level of Cyclin D expression that can induce cell division in the absence of *bmal1* repression.

See also Figure S6.

individually display an increased variance in the timing of $G_0$ release and a slight overall enhancement of proliferation (Figure 6F), cells stimulated at the same time in the LD cycle may have very different levels of p21 expression. Correspondingly, when averaged over a cell population, the timing of cell-cycle entry is more or less constant when measured at different ZTs (Figure S6C), and thus there is no phase dependency of M phase entry (Figure 6E). Although this is consistent with our experimental observations, further experiments will be needed to determine in greater detail how *mPer2* deletion impacts circadian rhythms in *bmal1* and CDK inhibitor expression.

## DISCUSSION

Our data indicate that the circadian clock regulates adult hippocampal neurogenesis by establishing a temporal window for QNPs to enter the cell cycle, and by setting the number of cell divisions prior to cell-cycle exit and terminal differentiation.

Components of the molecular-clock machinery are expressed in type 1 NSPCs of the adult SGZ. Genetic ablation of *Period2* abolishes the circadian gating of S phase entry of type 1 cells, revealing that cell-cycle entrance in the adult SGZ is regulated by the circadian clock. *Bmal1* deficiency, on the other hand, leads to a disproportionately high fraction of QNPs entering the cell cycle at all circadian times, and delays cell-cycle exit by additional rounds of cell division. Both effects likely contribute to the substantial increase in the number of newborn neurons in the DG of $bmal1^{-/-}$ mice. Most importantly, these results support the idea that the circadian clock not only temporally restricts the activation of QNPs but also buffers against overproduction of new neurons by limiting the number of QNPs that enter the cell cycle and the number of cell divisions that take place prior to cell-cycle exit.

Neurogenesis in the adult SGZ is characterized by differential expression of clock components. Similarly to the NSPCs of the adult subventricular zone (Kimiwada et al., 2009), quiescent

type 1 cells of the SGZ exhibit robust expression of core clock genes. However, unlike the quiescent state, the proliferative state is associated with a marked reduction in levels of BMAL1 and *period1/2* gene transcription. Strong expression of BMAL1 and *period1* is reinstated only after differentiation to granule neurons. In line with our findings, others have shown that in the thymus and testes, where the majority of cells are rapidly dividing, clock gene expression is noncyclic and at trough levels throughout the circadian cycle (Alvarez et al., 2003; Alvarez and Sehgal, 2005). However, it is not clear whether the onset of proliferation suppresses the circadian clock or the suppression of the circadian clock allows proliferation to occur.

Circadian rhythms in cell proliferation have been documented in multiple organisms (Dong et al., 2010; Bjarnason and Jordan, 2000). However, there is evidence that the exact relationship between the circadian clock and the cell cycle may be cell-type or context specific (Geyfman et al., 2012; Yeom et al., 2010; Gréchez-Cassiau et al., 2008; Matsuo et al., 2003). In agreement with several other reports (Matsumoto et al., 2011; Guzman-Marin et al., 2007), we found that overall proliferation in the adult SGZ exhibited a circadian rhythm, albeit with a low amplitude (1.3- to 1.6-fold). However, when we focused solely on type 1 cells (which express core clock genes at robust levels), the circadian variation in the number of these cells in S phase was found to be much greater in amplitude (∼2.5-fold). These results are similar to previous observations made in the skin, where the interfollicular epidermis exhibits a much more robust circadian rhythm of cell proliferation than the more actively proliferating early anagen hair follicle (Geyfman et al., 2012). The low-amplitude rhythms observed in the total population of proliferating cells in the SGZ may be the result of phase dispersion among cells that are in different cell-division cycles following clock suppression.

Significantly, our data show that the circadian clock influences the cell cycle during adult hippocampal neurogenesis in two ways. First, it restricts the overall number of QNPs that enter the cell cycle and the timing of entrance. In this regard, PER2 plays a specific role in the temporal regulation of cell-cycle entry, since loss of its expression ablates rhythmicity in population-level proliferation without significantly altering the number of actively cycling type 1 cells over a 24 hr period. In contrast, BMAL1 appears to be essential not only for maintaining rhythmicity in cell-cycle entry of QNPs but also for suppressing the number of type 1 cells that leave the quiescent state and proliferate. Other studies have suggested a direct link between components of the molecular clock and regulators of cell-cycle progression (e.g., *wee1* and p21) (Gréchez-Cassiau et al., 2008; Matsuo et al., 2003).

Second, the circadian clock impacts neurogenesis by modulating the number of cell divisions that occur before cells exit the cell cycle and complete the differentiation process. Our data show that in the absence of *bmal1*, cells are more prone to reenter the cell cycle, suggesting that more divisions are undertaken prior to their withdrawal from the cell cycle. We demonstrate the potential role of the circadian clock as a counting mechanism of cell-division events.

Importantly, we show that our experimental observations related to cell-cycle entry and exit are consistent with a mathematical model describing the modulation of cell-cycle progression by the circadian clock. The model assumes that cell-cycle entry is triggered when a mitogenic signal that induces Cyclin D expression surmounts a threshold that is set by the quiescent cell. This threshold is regulated by the circadian clock and fluctuates as a function of time-of-day, making it more likely that cells will enter the cell cycle at a particular ZT when the threshold is lower. It is not clear how the mitogenic signal is generated or how the circadian clock establishes a time-varying mitogenic threshold. Nonetheless, by assuming that the circadian clock enhances the expression of a CDK inhibitor such as p21 targeting cyclin D/Cdk4-6 (Laranjeiro et al., 2013), our model provides a simple explanation for how the circadian clock can gate cell-cycle entry by modulating the likelihood that cells will be released from quiescence.

A key element of our model is that clock suppression is an essential component of neurogenesis because it allows cells to be released from quiescence at lower mitogen stimulation. In the model, mitogen-mediated suppression of the clock provides a mechanism that allows Cyclin D/Cdk4-6 to become active and trigger S phase entry. Although other mechanisms are possible, clock suppression allowed us to reproduce the observations that cell-cycle entry varies with the time of day, that this dependency is abolished when *bmal1* is deleted, and that *bmal1* null cells are more likely to enter the cell cycle. Moreover, mitogen-mediated suppression of the clock may be important for explaining the relatively fast (<24 hr) cell-division cycle of the proliferating cells.

Clock suppression is also critical for the timing of cell-cycle exit. We assumed that cell-cycle exit is a consequence of a gradual cellular adaptation to the mitogen signal, leading to a gradual decrease in Cyclin D expression and a gradual increase in CDK inhibitor expression that eventually reestablishes the quiescent state. This is sufficient to explain why the timing of the return to quiescence is clock dependent: in the absence of *bmal1* and clock-activated expression of CDK inhibitors, cells can have sufficient time to complete four divisions, rather than two or three, before becoming mitogen insensitive. The model may also explain the observed essential role of mPER2 for temporally restricting cell-cycle entry during parts of the 24 hr LD cycle. One possibility is that PER function is essential for oscillations in the expression of clock-dependent CDK inhibitors. Another, simpler explanation is that mPER2 is essential for synchronizing the circadian clock oscillations among cells. In the model, a loss of PER function causes a loss of the entrainment to the LD cycle. In the absence of such synchronization, the expression of clock-dependent CDK inhibitors is uncoupled from the LD cycle, and the frequency with which cells enter the cell cycle is predicted to be constant.

In conclusion, our study shows that the circadian clock plays an important role in adult hippocampal neurogenesis by regulating the timely entry of NSPCs into the cell cycle and the number of cell divisions that take place prior to cell-cycle exit. Our work also raises the possibility that the circadian clock restricts the number of NSPCs that become activated to enter the cell cycle, thereby preventing premature exhaustion of the neural stem cell pool. The mathematical model provides a foundation for understanding potential interactions between the circadian clock and the cell cycle. Future investigations should

help to define the molecular-level mechanisms that govern the coupling between the circadian clock and the cell cycle as it pertains to adult hippocampal neurogenesis.

## EXPERIMENTAL PROCEDURES

### Animals

$Bmal1^{-/-}$ ($Arntl^{tm1Bra}$; Bunger et al., 2000), $period2^{-/-}$ ($Per2^{tm1Brd}$; Zheng et al., 1999), $Period2$::DsRed (Cheng et al., 2009), and $Period1$::VENUS (Cheng et al., 2009) mouse strains were used in this study. Data obtained from C57BL6/J mice (The Jackson Laboratory) were pooled with those obtained from $bmal1^{+/+}$ and $per2^{+/+}$ mice generated by heterozygous intercrosses and used as wild-type controls, since experiments showed no phenotypic difference in cell proliferation among the three wild-type groups. All animal handling and experimental procedures were conducted at the University of Toronto Mississauga animal facility, and approved by the local animal care committee in compliance with institutional guidelines and the Canadian Council on Animal Care.

### Thymidine Analog Injections

To analyze rhythms in cellular proliferation under entrained conditions, mice were maintained on an LD cycle, injected i.p. with BrdU (100 mg/kg; Sigma-Aldrich), and killed 6 hr later for tissue harvest. For proliferation rhythms under free-running conditions and cell-cycle entry of type 1 NSPCs, mice were transferred to DD for two cycles prior to a single BrdU injection at the prescribed ZT and tissues were harvested 3 hr later. For Figure 2, data for ZT 3, 9, 15, and 21 were collected during the manuscript revision stage and compiled with previously collected data for ZT 0, 6, 12, and 18. For some of the original ZTs (0, 6, 12, and 18), more mice were included to revalidate the initial findings. For cell-cycle exit analysis, mice were maintained on an LD cycle, injected with BrdU at ZT 12, and killed 24 hr later. Analysis of cell-cycle kinetics was performed as previously described (Brandt et al., 2012) with the following modifications: on the second day of release into DD, mice were injected with equimolar doses of 5-iodo-2′-deoxyuridine (IdU, 57.5 mg/kg; Sigma-Aldrich) and 5-chloro-2′-deoxyuridine (CldU, 42.5 mg/kg; Sigma-Aldrich). IdU was injected at ZT 8, and CldU was given either 4 hr (to determine S phase length) or 18 hr (to determine cell-cycle length) after IdU injection. Tissues were harvested 45 min after CldU injection. For LRC experiments, mice were maintained on an LD cycle and received a daily injection of BrdU at ZT 2 for 7 consecutive days. Tissues were harvested 30 days after the first injection.

### Immunohistochemistry and Immunofluorescence

BrdU immunohistochemistry (IHC) was performed as previously described (Choi et al., 2008) with minor modifications. IdU/CldU immunofluorescence (IF) detection was carried out according to previously described methods (Brandt et al., 2012). All other IF stains were performed using a standard protocol described elsewhere (Alvarez-Saavedra et al., 2011).

### Imaging

Images were acquired using a Zeiss Axio Observer Z1 inverted microscope equipped with a Laser Scanning Microscope (LSM) 700 module (for confocal image acquisition) and an AxioCam MRm Rev.3 monochromatic digital camera (for acquisition of bright-field images; Zeiss), along with the ZEN 2010 software. For each experiment, identical settings (including light intensity for IHC, gain, pinhole size, etc.) were used to acquire images of all samples.

### Quantification

Each experiment was performed using three 30 μm coronal sections of the medial hippocampus. The total number of single-, double-, and triple-stained cells was quantified using ImageJ software (http://rsbweb.nih.gov/ij) and the Cell Counter Plugins. BMAL1, $Per1$-VENUS, and $Per2$-DsRED expression levels were quantified in randomly selected Ki67$^+$ and Ki67$^-$ cells (ten each).

### Behavioral Analysis

#### DNMP-RAM Test

Mice were ~40 days old at the onset of the DNMP-RAM test and had been maintained on a reverse LD cycle for 2 weeks prior to testing. The test was conducted during the animals' active phase under dim red light according to previously described methods (Guo et al., 2011; Clelland et al., 2009).

#### Buried-Food Test

To assess olfaction, the buried-food test was conducted as previously described (Yang and Crawley, 2009) using Pirouline cream-filled wafers as palatable food.

#### Elevated Plus Maze

Anxiety was assessed using the elevated plus maze as described previously (Guo et al., 2004).

#### Object-Recognition Test

To assess performance on a hippocampus-independent cognitive process, we subjected mice to a short-term object-recognition test as previously described (Barker et al., 2007).

### Mathematical Simulations

Model simulations were conducted in MATLAB using ordinary differential equations (ODEs) and parameter definitions copied from source codes provided by C. Gérard (Gérard and Goldbeter, 2012). In the original model, expression of p21 contributes to a single variable representing a pool of CDK inhibitors with regulatory functions in all cell-cycle phases. In our model, p21 is described by its own variable and specifically inhibits the activity of Cyclin D/Cdk4-6. We assume that nuclear BMAL1 activates p21 expression and that the transcription of $bmal1$ is repressed by mitogen stimulation. We also modified the kinetics of AP1-modulated Cyclin D expression, and adjusted the parameter values to obtain a cell-cycle period of ~20 hr and to increase the robustness of cell-cycle progression.

We modeled mitogen stimulation and adaptation as a process that is independent of the cell cycle and the circadian clock by introducing a time dependency to the growth-factor parameter of the original model. The signal is simulated by maintaining the mitogen at a constant value for 30 hr poststimulation, followed by an exponential decay with a 12 hr half-life. We simulated the effect of $bmal1$ ablation by setting the rate of $bmal1$ transcription to zero. Like the CDK inhibitors, the original model uses single variables to represent the mRNA and protein abundances of all $period$ genes. Correspondingly, we simulated the effect of $mPer2$ deletion by reducing the transcription rate of the pooled $period$ genes by 40%. Smaller or greater reductions, as well as complete ablation of $period$ gene expression, yielded qualitatively similar results.

Simulations were done in two steps. First, the ODEs were integrated without mitogen stimulation until cyclin- and CDK-associated variables (except p21) reached a steady state. A 12:12 LD cycle was used to obtain a 24 hr circadian clock period. Second, the ODEs were integrated for a prestimulation period of up to 10 days and a poststimulation period of up to 7 days.

Oscillations in relative Cyclin B/Cdk1 activity were used to monitor proliferation and cell divisions. We assumed that the G2/M phase transition is defined by a peak in the activity of Cyclin B/Cdk1, and that cell division occurs once Cyclin B/Cdk1 is inactivated and its relative activity drops below 10%. Because simulated $mPer2$ ablation causes a loss of entrainment of the circadian clock to the LD cycle, we determined the dependency of cell proliferation on ZT in the $mPer2$-deficient mice by averaging the results of simulations in which mitogen stimulations occurred at the same point in the 12:12 LD cycle over 10 consecutive days.

The parameter threshold values required to induce cell proliferation were determined by Newton iteration. For each parameter guess, simulations were conducted as described above. A cutoff time of 48 hr poststimulation was imposed. A parameter guess was deemed "high" if mitogen stimulation failed to initiate a pulse in Cyclin B/Cdk1 activity during this period, and "low" otherwise. The value halfway between "low" and "high" was used as the next parameter guess.

Correspondence regarding the mathematical simulations should be addressed to mkaern@uottawa.ca.

### Statistical Analysis

One- and two-way ANOVAs of independent and repeated measures were used to analyze data, followed by post hoc Fisher's least-significant-difference tests with alpha set at <0.05. Statistical analyses were performed with statistical tools from StatView software version 4.57 (Abacus Concepts).

## REFERENCES

Altman, J., and Das, G.D. (1965). Autoradiographic and histological evidence of postnatal hippocampal neurogenesis in rats. J. Comp. Neurol. 124, 319–335.

Alvarez, J.D., and Sehgal, A. (2005). The thymus is similar to the testis in its pattern of circadian clock gene expression. J. Biol. Rhythms 20, 111–121.

Alvarez, J.D., Chen, D., Storer, E., and Sehgal, A. (2003). Non-cyclic and developmental stage-specific expression of circadian clock proteins during murine spermatogenesis. Biol. Reprod. 69, 81–91.

Alvarez-Saavedra, M., Antoun, G., Yanagiya, A., Oliva-Hernandez, R., Cornejo-Palma, D., Perez-Iratxeta, C., Sonenberg, N., and Cheng, H.Y. (2011). miRNA-132 orchestrates chromatin remodeling and translational control of the circadian clock. Hum. Mol. Genet. 20, 731–751.

Barker, G.R., Bird, F., Alexander, V., and Warburton, E.C. (2007). Recognition memory for objects, place, and temporal order: a disconnection analysis of the role of the medial prefrontal cortex and perirhinal cortex. J. Neurosci. 27, 2948–2957.

Bjarnason, G.A., and Jordan, R. (2000). Circadian variation of cell proliferation and cell cycle protein expression in man: clinical implications. Prog. Cell Cycle Res. 4, 193–206.

Brandt, M.D., Hübner, M., and Storch, A. (2012). Brief report: Adult hippocampal precursor cells shorten S-phase and total cell cycle length during neuronal differentiation. Stem Cells 30, 2843–2847.

Bunger, M.K., Wilsbacher, L.D., Moran, S.M., Clendenin, C., Radcliffe, L.A., Hogenesch, J.B., Simon, M.C., Takahashi, J.S., and Bradfield, C.A. (2000). Mop3 is an essential component of the master circadian pacemaker in mammals. Cell 103, 1009–1017.

Bunger, M.K., Walisser, J.A., Sullivan, R., Manley, P.A., Moran, S.M., Kalscheur, V.L., Colman, R.J., and Bradfield, C.A. (2005). Progressive arthropathy in mice with a targeted disruption of the Mop3/Bmal-1 locus. Genesis 41, 122–132.

Cheng, H.Y., Alvarez-Saavedra, M., Dziema, H., Choi, Y.S., Li, A., and Obrietan, K. (2009). Segregation of expression of mPeriod gene homologs in neurons and glia: possible divergent roles of mPeriod1 and mPeriod2 in the brain. Hum. Mol. Genet. 18, 3110–3124.

Choi, Y.S., Cho, H.Y., Hoyt, K.R., Naegele, J.R., and Obrietan, K. (2008). IGF-1 receptor-mediated ERK/MAPK signaling couples status epilepticus to progenitor cell proliferation in the subgranular layer of the dentate gyrus. Glia 56, 791–800.

Clelland, C.D., Choi, M., Romberg, C., Clemenson, G.D., Jr., Fragniere, A., Tyers, P., Jessberger, S., Saksida, L.M., Barker, R.A., Gage, F.H., and Bussey, T.J. (2009). A functional role for adult hippocampal neurogenesis in spatial pattern separation. Science 325, 210–213.

Dong, G., Yang, Q., Wang, Q., Kim, Y.I., Wood, T.L., Osteryoung, K.W., van Oudenaarden, A., and Golden, S.S. (2010). Elevated ATPase activity of KaiC applies a circadian checkpoint on cell division in Synechococcus elongatus. Cell 140, 529–539.

Encinas, J.M., Michurina, T.V., Peunova, N., Park, J.H., Tordo, J., Peterson, D.A., Fishell, G., Koulakov, A., and Enikolopov, G. (2011). Division-coupled astrocytic differentiation and age-related depletion of neural stem cells in the adult hippocampus. Cell Stem Cell 8, 566–579.

Gérard, C., and Goldbeter, A. (2009). Temporal self-organization of the cyclin/Cdk network driving the mammalian cell cycle. Proc. Natl. Acad. Sci. USA 106, 21643–21648.

Gérard, C., and Goldbeter, A. (2012). Entrainment of the mammalian cell cycle by the circadian clock: modeling two coupled cellular rhythms. PLoS Comput. Biol. 8, e1002516.

Geyfman, M., Kumar, V., Liu, Q., Ruiz, R., Gordon, W., Espitia, F., Cam, E., Millar, S.E., Smyth, P., Ihler, A., et al. (2012). Brain and muscle Arnt-like protein-1 (BMAL1) controls circadian cell proliferation and susceptibility to UVB-induced DNA damage in the epidermis. Proc. Natl. Acad. Sci. USA 109, 11758–11763.

Gréchez-Cassiau, A., Rayet, B., Guillaumond, F., Teboul, M., and Delaunay, F. (2008). The circadian clock component BMAL1 is a critical regulator of p21WAF1/CIP1 expression and hepatocyte proliferation. J. Biol. Chem. 283, 4535–4542.

Guo, M., Wu, C.F., Liu, W., Yang, J.Y., and Chen, D. (2004). Sex difference in psychological behavior changes induced by long-term social isolation in mice. Prog. Neuropsychopharmacol. Biol. Psychiatry 28, 115–121.

Guo, W., Allan, A.M., Zong, R., Zhang, L., Johnson, E.B., Schaller, E.G., Murthy, A.C., Goggin, S.L., Eisch, A.J., Oostra, B.A., et al. (2011). Ablation of Fmrp in adult neural stem cells disrupts hippocampus-dependent learning. Nat. Med. 17, 559–565.

Guzman-Marin, R., Suntsova, N., Bashir, T., Szymusiak, R., and McGinty, D. (2007). Cell proliferation in the dentate gyrus of the adult rat fluctuates with the light-dark cycle. Neurosci. Lett. 422, 198–201.

Jin, K., Zhu, Y., Sun, Y., Mao, X.O., Xie, L., and Greenberg, D.A. (2002). Vascular endothelial growth factor (VEGF) stimulates neurogenesis in vitro and in vivo. Proc. Natl. Acad. Sci. USA 99, 11946–11950.

Kempermann, G., Kuhn, H.G., and Gage, F.H. (1997). More hippocampal neurons in adult mice living in an enriched environment. Nature 386, 493–495.

Kimiwada, T., Sakurai, M., Ohashi, H., Aoki, S., Tominaga, T., and Wada, K. (2009). Clock genes regulate neurogenic transcription factors, including NeuroD1, and the neuronal differentiation of adult neural stem/progenitor cells. Neurochem. Int. 54, 277–285.

Kippin, T.E., Martens, D.J., and van der Kooy, D. (2005). p21 loss compromises the relative quiescence of forebrain stem cell proliferation leading to exhaustion of their proliferation capacity. Genes Dev. 19, 756–767.

Kuhn, H.G., Dickinson-Anson, H., and Gage, F.H. (1996). Neurogenesis in the dentate gyrus of the adult rat: age-related decrease of neuronal progenitor proliferation. J. Neurosci. 16, 2027–2033.

Laranjeiro, R., Tamai, T.K., Peyric, E., Krusche, P., Ott, S., and Whitmore, D. (2013). Cyclin-dependent kinase inhibitor p20 controls circadian cell-cycle timing. Proc. Natl. Acad. Sci. USA 110, 6835–6840.

Leloup, J.C., and Goldbeter, A. (2004). Modeling the mammalian circadian clock: sensitivity analysis and multiplicity of oscillatory mechanisms. J. Theor. Biol. *230*, 541–562.

Marqués-Torrejón, M.Á., Porlan, E., Banito, A., Gómez-Ibarlucea, E., Lopez-Contreras, A.J., Fernández-Capetillo, O., Vidal, A., Gil, J., Torres, J., and Fariñas, I. (2013). Cyclin-dependent kinase inhibitor p21 controls adult neural stem cell expansion by regulating Sox2 gene expression. Cell Stem Cell *12*, 88–100.

Matsumoto, Y., Tsunekawa, Y., Nomura, T., Suto, F., Matsumata, M., Tsuchiya, S., and Osumi, N. (2011). Differential proliferation rhythm of neural progenitor and oligodendrocyte precursor cells in the young adult hippocampus. PLoS ONE *6*, e27628.

Matsuo, T., Yamaguchi, S., Mitsui, S., Emi, A., Shimoda, F., and Okamura, H. (2003). Control mechanism of the circadian clock for timing of cell division in vivo. Science *302*, 255–259.

Mira, H., Andreu, Z., Suh, H., Lie, D.C., Jessberger, S., Consiglio, A., San Emeterio, J., Hortigüela, R., Marqués-Torrejón, M.A., Nakashima, K., et al. (2010). Signaling through BMPR-IA regulates quiescence and long-term activity of neural stem cells in the adult hippocampus. Cell Stem Cell *7*, 78–89.

Parent, J.M., Yu, T.W., Leibowitz, R.T., Geschwind, D.H., Sloviter, R.S., and Lowenstein, D.H. (1997). Dentate granule cell neurogenesis is increased by seizures and contributes to aberrant network reorganization in the adult rat hippocampus. J. Neurosci. *17*, 3727–3738.

Seri, B., García-Verdugo, J.M., McEwen, B.S., and Alvarez-Buylla, A. (2001). Astrocytes give rise to new neurons in the adult mammalian hippocampus. J. Neurosci. *21*, 7153–7160.

Song, J., Zhong, C., Bonaguidi, M.A., Sun, G.J., Hsu, D., Gu, Y., Meletis, K., Huang, Z.J., Ge, S., Enikolopov, G., et al. (2012). Neuronal circuitry mechanism regulating adult quiescent neural stem-cell fate decision. Nature *489*, 150–154.

van Praag, H., Kempermann, G., and Gage, F.H. (1999). Running increases cell proliferation and neurogenesis in the adult mouse dentate gyrus. Nat. Neurosci. *2*, 266–270.

Yang, M., and Crawley, J.N. (2009). Simple behavioral assessment of mouse olfaction. Curr. Protoc. Neurosci. *Chapter 8*, 24.

Yeom, M., Pendergast, J.S., Ohmiya, Y., and Yamazaki, S. (2010). Circadian-independent cell mitosis in immortalized fibroblasts. Proc. Natl. Acad. Sci. USA *107*, 9665–9670.

Zheng, B., Larkin, D.W., Albrecht, U., Sun, Z.S., Sage, M., Eichele, G., Lee, C.C., and Bradley, A. (1999). The mPer2 gene encodes a functional component of the mammalian circadian clock. Nature *400*, 169–173.